



This is a repository copy of *Optimizing size and distribution of voids in phenolic resins through the choice of catalyst types*.

White Rose Research Online URL for this paper:  
<https://eprints.whiterose.ac.uk/148673/>

Version: Published Version

---

**Article:**

Hamad, S.F., Farr, N., Fei, T. et al. (5 more authors) (2019) Optimizing size and distribution of voids in phenolic resins through the choice of catalyst types. *Journal of Applied Polymer Science*, 136 (47). 48249. ISSN 0021-8995

<https://doi.org/10.1002/app.48249>

---

**Reuse**

This article is distributed under the terms of the Creative Commons Attribution (CC BY) licence. This licence allows you to distribute, remix, tweak, and build upon the work, even commercially, as long as you credit the authors for the original work. More information and the full terms of the licence here:  
<https://creativecommons.org/licenses/>

**Takedown**

If you consider content in White Rose Research Online to be in breach of UK law, please notify us by emailing [eprints@whiterose.ac.uk](mailto:eprints@whiterose.ac.uk) including the URL of the record and the reason for the withdrawal request.



[eprints@whiterose.ac.uk](mailto:eprints@whiterose.ac.uk)  
<https://eprints.whiterose.ac.uk/>

## Optimizing size and distribution of voids in phenolic resins through the choice of catalyst types

Sameer F. Hamad <sup>1,2</sup> Nicholas Farr,<sup>1</sup> Teng Fei,<sup>1</sup> Nur F. Shukor,<sup>1</sup> Julian S. Dean,<sup>1</sup> Simon A. Hayes,<sup>3</sup> Joel P. Foreman,<sup>1</sup> Cornelia Rodenburg<sup>1</sup>

<sup>1</sup>Department of Materials Science and Engineering, The University of Sheffield, Sheffield S1 3JD, UK

<sup>2</sup>College of Engineering, University of Misan, Maysan 62001, Iraq

<sup>3</sup>Department of Multidisciplinary Engineering Education, The University of Sheffield, Sheffield S3 7RD, UK

Correspondence to: S. F. Hamad (E-mail: sfhamad1@sheffield.ac.uk or sfhamad3@gmail.com)

**ABSTRACT:** Phenolics are widely used for over a century in different industries due to their chemical resistance and thermomechanical properties. However, the presence of voids in phenolic resins has negative effects on the mechanical properties and a conventional approach is to avoid these by utilizing very long cure cycles. Our alternative approach investigates the tailoring of void size and distribution to achieve a better balance between processing time and mechanical properties. Therefore, we produced phenolic resin with a void-free microstructure by a long cure cycle as a reference. To alter the void size and distributions, we utilized different catalysts and a short cure cycle to obtain phenolic resins and test their flexural properties with respect to the reference. We investigated the fracture surfaces of all materials by SEM, FTIR and compared results to finite element modeling that confirmed the effects of different void size and distributions on the mechanical properties. © 2019 The Authors. *Journal of Applied Polymer Science* published by Wiley Periodicals, Inc. *J. Appl. Polym. Sci.* **2019**, *136*, 48249.

**KEYWORDS:** mechanical properties; microscopy; morphology; porous materials; thermosets

Received 28 April 2019; accepted 2 June 2019

DOI: [10.1002/app.48249](https://doi.org/10.1002/app.48249)

### INTRODUCTION

Phenolics or phenol-formaldehyde resins are amongst the oldest thermosetting polymers, with excellent ablative properties, low smoke density, high chemical resistance, and thermal stability.<sup>1–5</sup> Such resins have been used in a broad range of applications such as molding compounds, thermal insulation materials, coatings, laminates, wood products industry, and structural adhesives,<sup>6,7</sup> and most of all as light weight foams in aerospace applications.<sup>8,9</sup> Furthermore, phenolics are also utilized as a matrix material for composite applications in the sport and construction industries due to their capability of withstanding highly corrosive environments.<sup>10</sup> However, it might be seen surprising even nowadays phenolic resins still suffer from the slow crosslinking rate and the high curing temperature.<sup>11</sup> Moreover, the mechanical properties of phenolic resins can be compromised by porosity and how to control it to a desired level still poses a scientific and industrial challenge.<sup>12</sup> The reason for this is the long and complex polymerization process together with the generation of water and formaldehyde as by

products. Void-free phenolic parts usually require long heating cycles,<sup>13</sup> thus not only taking a long time to produce but their production is also energy intensive. Here, we investigate how to minimize any loss in mechanical properties as a consequence of implementing a short curing cycle.

Phenolic resins are produced from the polycondensation reaction of the phenol and formaldehyde. Based on the formaldehyde/phenol molar ratios and curing properties, phenolic resin is characterized into two main categories: novolac and resole resins.<sup>14–16</sup> Generally, both cured phenolic resin types (novolac and resole) are almost identical in terms of mechanical properties and chemical resistance.<sup>17</sup> Novolacs are synthesized in the presence of an acid catalyst with an excess of phenol and do not react further without a curing agent. Hence, to produce a crosslinked structure of novolac resin, curing agents such as hexamethylenetetramine (HMTA) must be added.<sup>17</sup> However, the resin of interest for liquid molding is resole resin.<sup>16</sup> Resoles are prepared in the presence of an alkaline catalyst with an excess of formaldehyde, producing a soluble and

Additional Supporting Information may be found in the online version of this article.

© 2019 The Authors. *Journal of Applied Polymer Science* published by Wiley Periodicals, Inc.

This is an open access article under the terms of the Creative Commons Attribution License, which permits use, distribution and reproduction in any medium, provided the original work is properly cited.

fusible prepolymer. Resole structures contain reactive hydroxymethyl groups and by heating, a crosslinked structure can be produced.<sup>17</sup>

During the crosslinking of the phenol-formaldehyde resin, the release of the by-products becomes very difficult as the resin viscosity rises.<sup>18</sup> Consequently, the presence of these by-products in the cured resin can lead to porosity in the form of macro<sup>13</sup> or microvoids (8–10  $\mu\text{m}$  in size),<sup>16</sup> which adversely affects the mechanical properties of the final cured resin.<sup>16</sup> However, it has been reported that phenolic resin with void-free microstructures could be produced if the gelation time is kept long enough for the water vapor to be released.<sup>13,19</sup> This approach requires a very long heat cure cycle, which is not favorable for most industries due to time and energy consumption issues. Therefore, there have been many attempts to accelerate the crosslinking rate of the phenolic resins with the use of different curing agents<sup>20–23</sup> but in each case, the formation of voids cannot be avoided.

No existing approaches allow void-free microstructures to be achieved with a short cure cycle, therefore, a novel approach to optimize the microvoids size and distribution in a fast curing process for better mechanical properties at minimum processing time is proposed as an alternative. This investigation is inspired by the observation that in phenolic foams with deliberately high void volumes, the void diameter and distribution do affect the mechanical properties in a way that is not predicted by any current models.<sup>24</sup> Not only the void volume fraction but void diameter and void distribution were empirically found to be of importance in determining the final mechanical properties. However, the void size distributions (100–450  $\mu\text{m}$ ) obtained in phenolic foams<sup>25</sup> are significantly larger than those in phenolics intended as bulk materials or as matrix for composite materials. For the latter group of materials, few studies have considered the effects of the void size and distribution on the final mechanical properties of the cured phenolic resins.<sup>26</sup> Most studies have focused on the investigation of the effects of formaldehyde/phenol (F/P) molar ratios,<sup>27–29</sup> reaction conditions (temperature and time),<sup>26</sup> degree of condensation,<sup>30</sup> catalyst concentrations,<sup>26</sup> and catalyst type<sup>31</sup> on the final properties of the cured resins. Here, we investigate the possibility of changing the catalyst type to tailor void size and distributions in order to enable fast resin curing, while minimizing the effect of voids on the mechanical properties in comparison to the reference sample.

The objective of this study is to investigate the optimum void size and diameter distribution as well as the spatial distribution of the voids in the phenolic produced in a fast curing process and compare their mechanical properties to a void-free reference phenolic. To this end a cross-linked resole phenolic resin material was produced using a long cure cycle (4 days) without the use of a catalyst. A slow action acid catalyst (Phencat 382) and a fast action acid catalyst (Phencat 10) were then utilized to produce two phenolic resin samples types with varying void sizes and distributions and mechanical properties (strength and modulus obtained from bending tests). To visualize and quantify detailed void structures, diameters and distributions, low voltage scanning electron microscopy (LV-SEM) was used to image the fractured surface of the above three types of cured phenolic resin. The latter enables the observation of highly localized variation in chemistry and crack behavior. To account for the effects introduced by the variation of average chemical composition all of the cured phenolic resins were subject to analysis by Fourier transform infrared (FTIR).

## EXPERIMENTAL

### Materials

In this study, a resole commercial phenolic resin called Cellobond J2027X was used (kindly supplied by Caleb Technical Products Ltd., UK). This kind of resin is usually available as a water-based controlled-viscosity resin, which can be cured either with the application of heat only (long cure cycle) or at lower temperature (60°C), short cure cycle (3 h), with the use of a strong acid catalyst.<sup>16</sup> It is suitable for the fabrication of fiber composites by hand layup and resin transfer molding.<sup>32</sup> Two types of catalyst (Cellobond Phencat 382 and Cellobond Phencat 10) supplied by the same company (Caleb Technical Products Ltd., UK) were used in this study. Phencat 382 is a relatively slow action acid catalyst (working life 4 h), which is activated at low temperature, typically 60–80 °C.<sup>16</sup> It is an acid-based catalyst consisting of phosphoric acid, C3-9-alkyl esters (75–90%), and phosphoric acid (10–25%) by weight. Phencat 10 is a general purpose catalyst for processes such as contact molding giving working life of about 20 min. It is a composition consists of p-toluenesulphonic acid (35–50%) and phosphoric acid (10–25%) by weight.

### Curing Process of Commercial Resole Phenolic Resin

Two different curing schedules were used to cure the resole phenolic resin:

- 1-. Long cure cycle, the as received resole phenolic resin was poured into a PTFE mold and then placed in an autoclave to be cured using the cure cycle as shown in Figure 1.
- 2-. Short cure cycle, the resole phenolic resin was first mixed with either slow action acid catalyst (phencat 382), or fast action acid catalyst (phencat 10), and then poured into the PTFE mold to be placed in an autoclave using a short cure cycle as shown in Table I. The catalyst ratio was maintained at 5 wt% of the resin for all samples.

### Characterization

**Scanning Electron Microscopy SEM.** Scanning electron microscopy (FEI Nova Nano SEM 450) was used for the morphology observation of the fracture surface of the flexural strength samples. Unlike standard SEM analysis, no conductive coating was deposited onto the samples. Therefore, a low accelerating voltage (1 KV) was used to avoid sample surface charging and damage with typical vacuum pressure of  $10^{-5}$  mbar, and a working distance of about 4 mm. Secondary electron images were collected using either an Everhart–Thornley Detector (ETD) for low magnification images or a Through Lens Detector (TLD) to obtain high magnification images.

**Fourier Transform Infrared Spectroscopy.** The chemical composition of all cured phenolic resins was investigated using a PerkinElmer Frontier spectrometer. To prepare the FTIR sample pellet, 2 mg of sample powder (ground from the bulk sample) was diluted with 300 mg of spectroscopic grade KBr. The test was performed at room temperature ( $22 \pm 3^\circ\text{C}$ ) with a wavenumber range between 4000 and 600  $\text{cm}^{-1}$ , and the average of scan repetitions was 32 scans for each sample at 2  $\text{cm}^{-1}$  of resolution. Before loading the sample, a background spectrum was taken as a control.

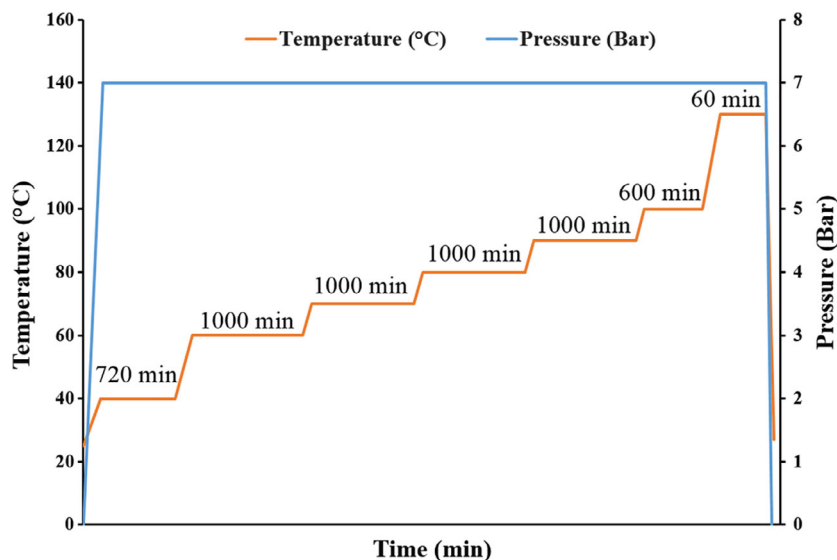


**Figure 1.** Long cure cycle used to cure phenolic resin without any catalyst. The heating ramp rate and pressure ramp rate were 2°C/min and 0.3 Bar/min, respectively. [Color figure can be viewed at [wileyonlinelibrary.com](http://wileyonlinelibrary.com)]

**Flexural Test.** The flexural properties (strength and modulus) of all specimens were determined using a Lloyd TA500 tensometer. The test was performed according to the ASTM D790 (standard test methods for flexural properties of unreinforced and reinforced plastics and electrical insulating materials) with a span to sample thickness ratio of 16. Crosshead speeds of all tests were 2.0 mm/min. The tests were performed at room temperature ( $22 \pm 3^\circ\text{C}$ ).

The ultimate bending results of each type of phenolic resin were calculated as an average of seven specimens per test condition. The flexural modulus was determined from the following formula:

$$E = \frac{L^3 F}{4 w h^3 d} \quad (1)$$

Where  $E$  is the modulus of elasticity in bending (MPa),  $L$  is the support span (mm),  $F$  is the peak load (N),  $w$  is the width of the sample (mm),  $h$  is the thickness (mm), and  $d$  is the sample deflection (mm).

## RESULTS AND DISCUSSION

### Fracture Surface Characterization

The fracture surfaces obtained by the bending test of the three types of cured phenolic resin were observed by LV-SEM and their micrographs are shown in Figure 2. A homogenous fracture

surface without any micron-sized voids was observed for the reference sample cured without catalyst, using the long cure cycle (Figure 1), as shown in Figure 2(a). A higher magnification image [Figure 2(b)] reveals the presence of a large number of bright nanostructures with diameters well below 100 nm. Their dimensions are consistent with previous electron microscopy studies of replicas of fractured phenolic resin surfaces.<sup>33</sup> These structures were interpreted as localized areas of increased crosslinking density<sup>33</sup> but the observed contrast would have been consistent with voids too. A few such bright nanostructures can be seen also in at the fracture surface of the specimens prepared with the slow action catalyst as shown in Figure 2(c,d). However, the latter fracture surfaces also show clear evidence of voids with diameters that reach from hundreds of nanometres to several micrometers. This is more easily seen in the diameter distribution histograms in Figure 3(a), which was derived from the binary images [Figure 4(a)]. Likewise, we present SEM images of the fracture surfaces obtained from materials produced with a fast action catalyst in Figure 2(e,f) and the respective diameter distribution histogram in Figure 3(b). The histogram was derived from the binary images presented in in Figure 4(b). The histogram [Figure 3(b)] shows clearly that the overwhelming majority of structures is of submicron size, with an average diameter of  $0.52 \pm 0.15 \mu\text{m}$ , while the SEM images demonstrates the dense and homogenous coverage [Figure 2 (f)] of the fracture surface with spherical features.

**Table I.** Short Cure Cycle Used to Cure Phenolic Resin With the Addition of Catalyst

Temperature (°C)	Temperature ramp rate (°C/min)	Pressure (Bar)	Pressure ramp rate (Bar/min)	Dwell time (min)
80	2.00	7.00	0.30	180
130	2.00	7.00	0.00	60
27	2.00	0.00	0.20	0.00

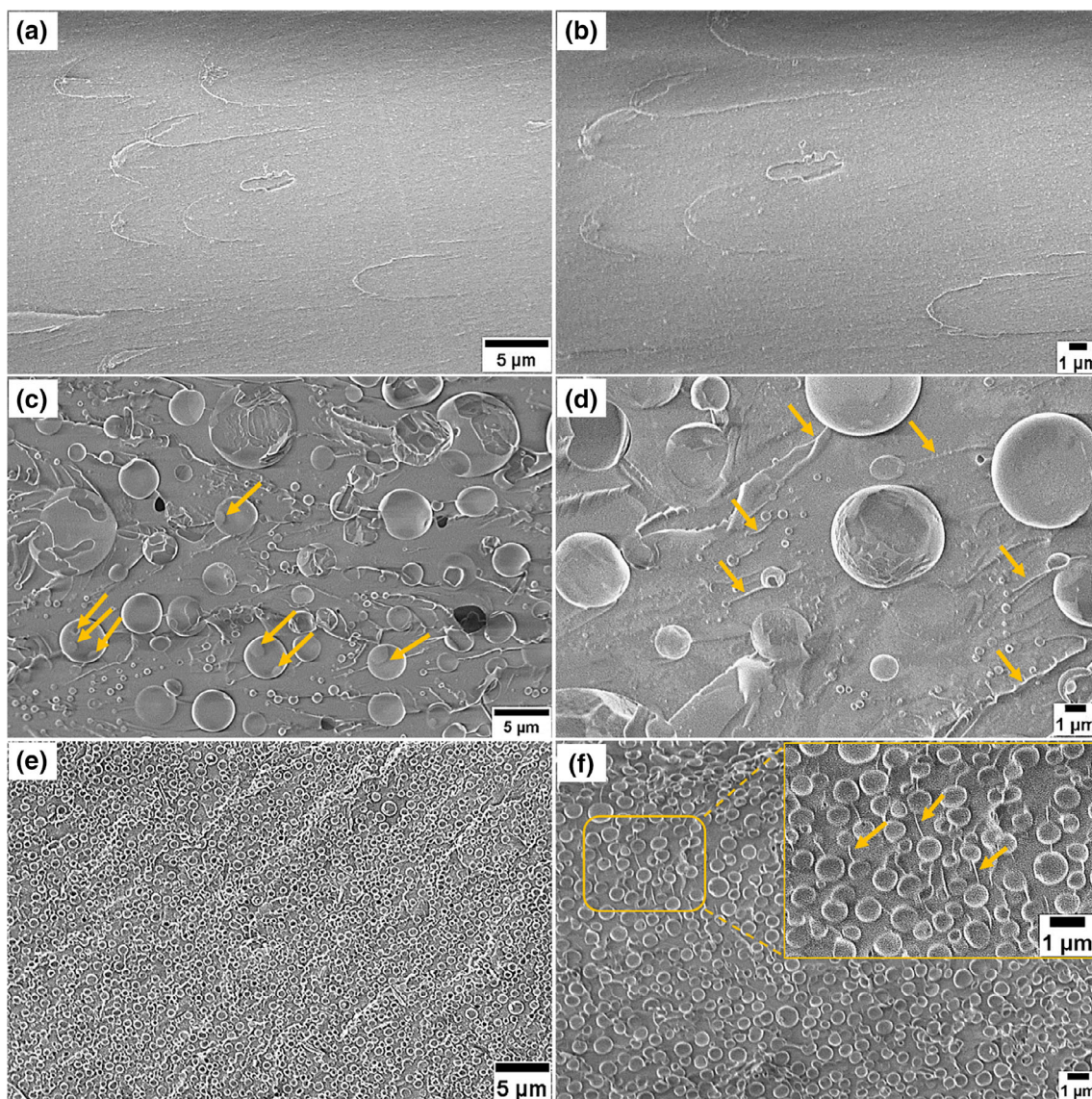


**Figure 2.** LV-SEM micrographs of the fracture surface of the three types of cured phenolic resins, (a) low and (b) high magnification images of phenolic resin cured using long cure cycle without added catalyst, (c) low and (d) high magnification images of phenolic resin cured with the addition of slow action catalyst (phencat 382), and (e) low and (f) high magnification images of phenolic resin cured with the addition of fast action catalyst (phencat 10). Arrows in (c) indicate the bubbles coalescence. Arrows in (d) and (f) (insert micrograph) indicate the cracks. [Color figure can be viewed at [wileyonlinelibrary.com](http://wileyonlinelibrary.com)]

To understand the origin of the patterns is worth noting that a combination of small-angle neutron scattering (SANS) and small-angle X-ray scattering (SAXS) experiment on phenolic resins revealed that rough interfaces between voids and phenolic matrix with a fractal dimensions  $\sim 2.46$  to  $2.6$  exist.<sup>34</sup> This fractal dimension is consistent with the existence of Apollonian arrangement for which a fractal dimensions of  $2.4739465$  was established.<sup>35</sup> Apollonian packing is found and used in the controlled preparation of ordered porous films exploiting Breath Figures, to produce so called Breath Figure arrays (BFA).<sup>36</sup> In BFA fabrication, the irregular pore arrays are observed if water droplet can coalesce, while homogenous pore arrays when the coalesce of water droplets can be prevented.

Therefore, all of the observations in Figure 2 can be understood in terms of time available before the gel point is reached. If this is long enough for the release of the water vapor before the start of

crosslinking in the resin structure,<sup>19</sup> the formation of voids can be prevented as is the case in the reference material [Figure 2(a)]. In contrast, with the use of catalysts, the crosslinking rate of the phenol-formaldehyde resins is relatively fast. As the amount of water in the resin increased during the reaction, molecular clusters can form that then nucleate when the saturation level at a given temperature and pressure is locally exceeded.<sup>12</sup> This leads to phase-separation and produces water domains.<sup>32</sup> With the fast action catalyst [Figure 2(e,f)], the crosslinking rate is very fast (only 20 min working life according to the technical data sheet), and the gelation time is very short. Therefore, the trapped water, present as a result of the complex polymerization process including the release of formaldehyde and water as by-products,<sup>37</sup> will not be able to be released or diffuse, resulting in a homogenous distribution of voids with the very narrow size distribution as seen in

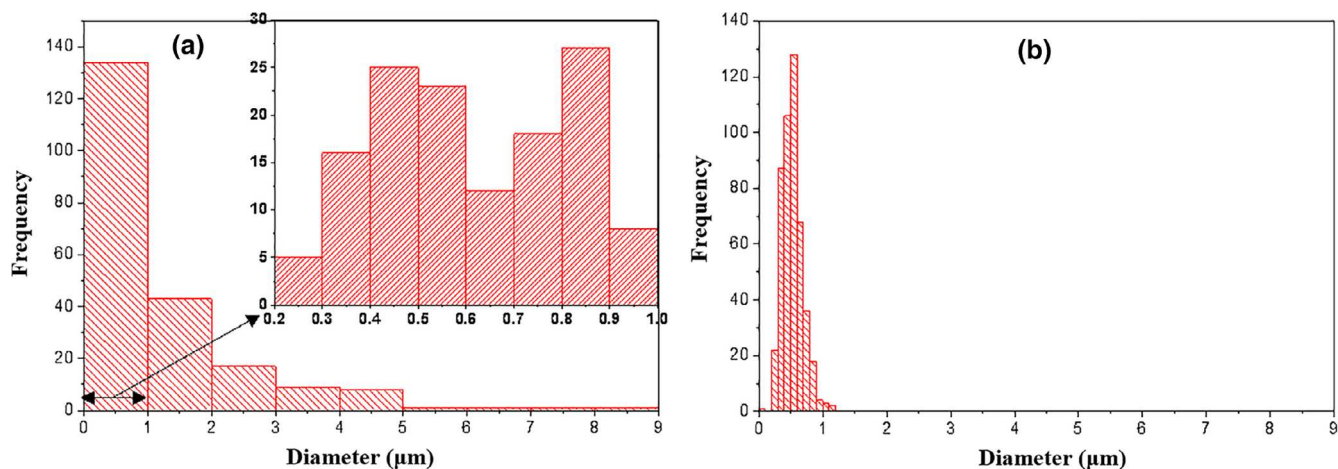


**Figure 3.** Histogram of voids diameter distribution: (a) phenolic resin cured with a slow action catalyst (phencat 382), and (b) phenolic resin cured with a fast action catalyst (phencat 10). [Color figure can be viewed at [wileyonlinelibrary.com](http://wileyonlinelibrary.com)]

Figure 3(b). In contrast, with the use of a slow action catalyst [material in Figure 2(c,d)], the cross linking rate is slower (4 h working life according to the technical data sheet), and the gelation time is longer. Therefore, the generated water can move and coalesce leading to the very broad size distribution of voids, as well as a wide variation in distances between voids. Larger voids tend to be surrounded by void-free zones as can be seen in the binary image and distance map in Figure 4(a). The distance between small voids in Figure 4(a) is similar to that found in the distance map obtained from the material made by the fast action catalyst [Figure 4(b)]. However, the distance to larger voids in Figure 4(a) is substantially larger than the distance in Figure 4(b).

The above is also reflected in Figure 4(c), which compares the distances between voids in the materials made using slow and

fast action catalysts, respectively. While for the slow action catalysts, distances between voids can exceed 4  $\mu\text{m}$ , the use of fast action catalyst results in distances between voids  $<1.5 \mu\text{m}$ . This difference is likely to play a critical role with regards to the mechanical properties, as the voids do seem to effect crack initiation and growth as evidenced by Figure 2(d,f) (indicated by arrows). Both figures contain the evidence of cracks (wide due to the edge effect). In the material produced from the slow action catalyst [Figure 2(d)] fewer but longer cracks are observed than in the material made with the fast action catalyst [Figure 2(f) (insert micrograph)]. The longest cracks in Figure 2(d) are found to propagate in the void-free zones with no clear termination point, while all of the cracks visible in Figure 2(f) (insert micrograph) are terminated at both ends by voids.

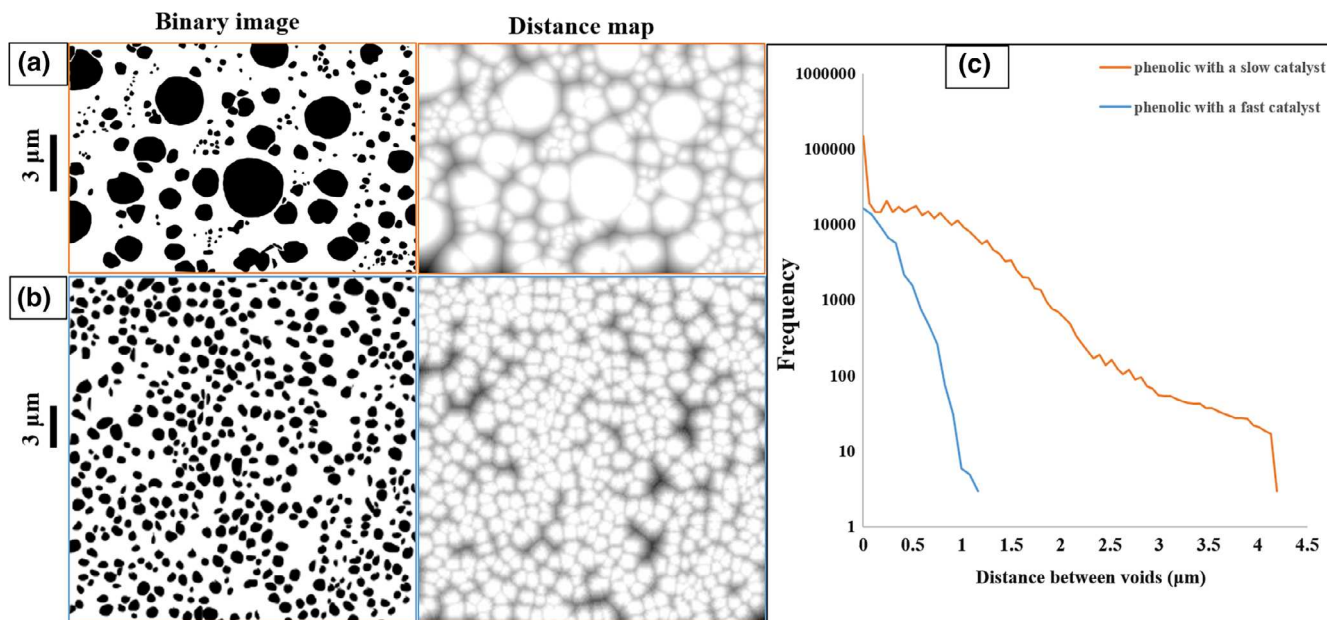


**Figure 4.** Voids analysis in phenolic resins cured with (a) a slow action catalyst, and (b) a fast action acid catalyst. (c) Histogram of intervoids distance for the images presented in (a) and (b). Image processing was performed using Fiji software.<sup>38</sup> [Color figure can be viewed at [wileyonlinelibrary.com](http://wileyonlinelibrary.com)]

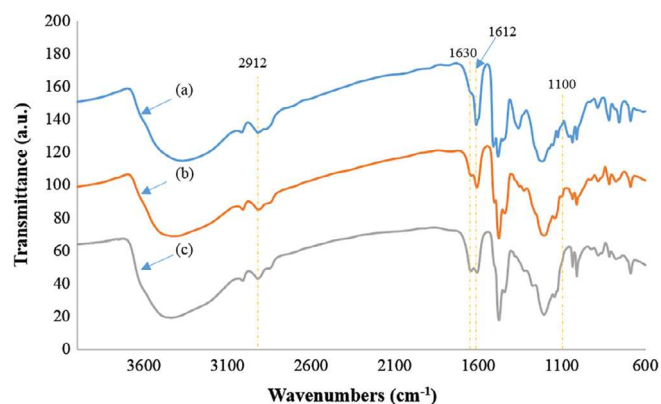


**Figure 5.** The IR spectrum of phenol/formaldehyde resin cured (a) without catalyst, (b) with a slow action catalyst (Phencat 382), and (c) with a fast action catalyst (Phencat 10). [Color figure can be viewed at [wileyonlinelibrary.com](http://wileyonlinelibrary.com)]

Further differences between the materials made using slow and fast action catalysts, respectively, is in the volume fraction taken up by the voids structures. We can only measure area fractions from the 2D SEM images (28% in materials from fast action catalyst & 33% in materials using slow action catalyst). However, the volume fraction is only directly proportional to the area fraction if the sectioning plane intersects the structural features at random. As are sections are produced by fracture the later condition is not necessarily fulfilled here, because as seen in Figure 2(d)

(indicated by arrows) wide cracks are seen to run along the larger voids. While all of the above will affect the mechanical properties (see sections 3.3 and 3.4 for full details), differences in chemistry as a result of using the different catalysts could also be responsible for the differences in mechanical properties.

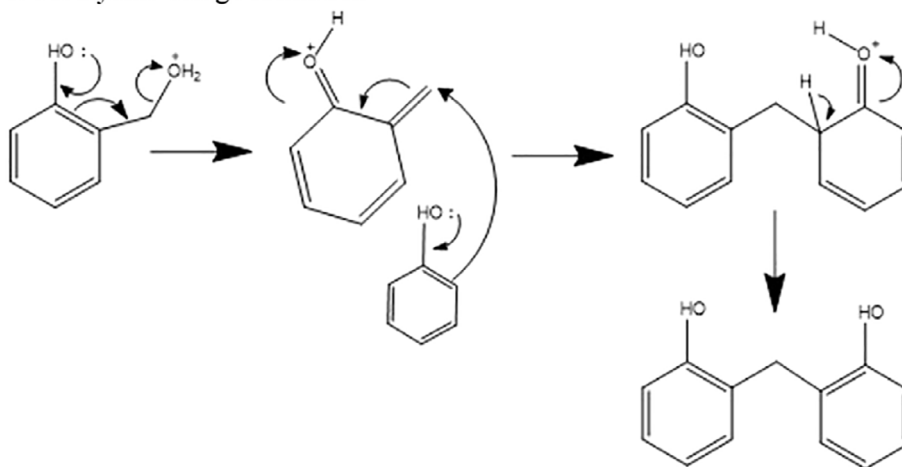
### The Chemical Composition Analysis

Results of FT-IR measurements are presented in Figure 5 in order to enable component identification of the products produced by the condensation reaction of phenol and formaldehyde. The standard peak positions<sup>39</sup> and the observed peaks of the resole phenol/formaldehyde resins are assigned in Supporting Information (Supporting Information Table S1).

It was expected that both catalysts used would be observable through two clear absorption bands; one band at  $1650\text{ cm}^{-1}$ , noted for hydrated phosphates P—OH and corresponding to O—H stretching and O—H deformation vibrations and second band between  $1300$  and  $900\text{ cm}^{-1}$  that is characteristic of P—O and C—O vibrations.<sup>40</sup> In this reaction, these absorption bands cannot be independently isolated as both bands coincide with the phenolic resin bands at  $1594\text{ cm}^{-1}$ , corresponding to the absorption of C=C of phenyl rings, and bands  $1100\text{ cm}^{-1}$ , which are the characteristic of the C—H flexural of phenyl rings.

Two bands observed at  $1630\text{ cm}^{-1}$  and  $1612\text{ cm}^{-1}$  are of particular interest. The first band was noted as the C = O stretch

### 1. Methylene bridge formation



### 2. Ether bridge formation

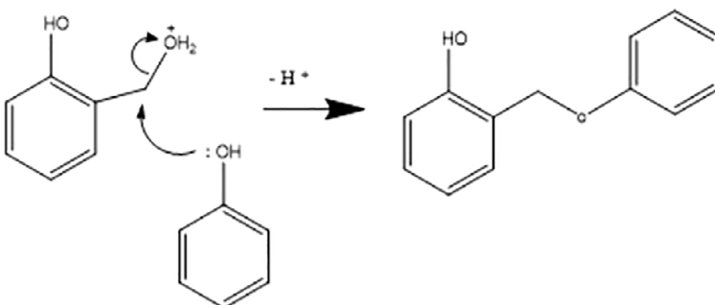


**Figure 6.** Two possible reactions of phenol/formaldehyde resin with acid catalyst.

**Table II.** Flexural Properties of The Three Types of Cured Phenolic Resins

Sample	Flexural strength (MPa)	STDEV	Flexural modulus (GPa)	STDEV	Deflection (mm)	STDEV
Phenolic without catalyst	88	18	3.2	0.28	1.2	0.25
Phenolic with slow action catalyst (382)	47	8	2.0	0.25	0.99	0.11
Phenolic with fast action catalyst (10)	68	12	2.3	0.43	1.2	0.25

(overlapped with OH scissors of water), which is the characteristic of unreacted formaldehyde. This first band has higher intensity when the materials is made using a catalyst with a short cure cycle when compared to phenolic cured without a catalyst using long cure cycle. This absorption band can be interpreted in either of the two ways: firstly, the resins formed using a catalyst might have a slightly reduced cross linking density or secondly, and more likely, the acid catalyst pushes the equilibrium of the two-step reaction toward the second step of the polymerization of phenolic resin. Either interpretation results in less formaldehyde being used in the initial reaction and thus leads to the presence of unreacted formaldehyde. The latter is more likely because it is observable that the phenolic resin cured with a fast action acid catalyst showed a stronger  $1630\text{ cm}^{-1}$  band when compared to that of phenolic resin cured with a slow action acid catalyst. This result would be expected as the fast catalyst is the more acidic.

An interesting feature is the absorption band present at  $1612\text{ cm}^{-1}$ . This absorption band displays a greater intensity in the case of phenolic resin cured without catalyst than that of either catalyst. The band is caused by the  $\text{C}=\text{C}$  aromatic ring within a functional group of phenol-formaldehyde resin. This is the product of the first step reaction of phenol and formaldehyde and therefore is consistent with the premise that the acid catalyst is slowing down the formation of this product.

Two interesting bands were also noted at  $2912\text{ cm}^{-1}$  and  $1100\text{ cm}^{-1}$ , these bands are attributed to methylene and ether bridges, respectively.<sup>39</sup> Changes in the two bands values were observed

between the two catalysts. These changes are expected to originate from the differences of the phenol-bonding mechanism. It was noted that there was a reduction of ether bridges within phenolic resin cured with a fast action catalyst when compared to that of phenolic resin cured with a slow action catalyst and a consequential increase in methylene bridges in phenolic cured with fast catalyst when compared to that of phenolic cured with slow catalyst. The more acidic the catalyst, the more that the phenol is protonated and therefore the less nucleophilic it is. As a result, it is less likely that it will follow a second mechanism and form ether bridges (see Figure 6). The results observed point to an increased likelihood that the first mechanism is the correct one. If so, the more acidic catalyst (fast action catalyst) will promote the formation of methylene bridges within the phenolic. Methylene bridges have a greater bond strength than that of ether bridges.<sup>41</sup> This can result in different mechanical properties of the phenolic due to more methylene bridges (see section 3.3).

### Flexural Strength and Modulus

The flexural properties of the three types of cured phenolic resins were determined and are presented in Table II. It can be seen that the phenolic resin cured without a catalyst, using a long cure cycle (almost 4 days), has the highest average values of flexural strength ( $88 \pm 18\text{ MPa}$ ) and modulus ( $3.2 \pm 0.28\text{ GPa}$ ) in comparison to those of phenolic resins cured with catalysts. This is expected and can be explained in part by the reduced area of phenolic resin due to the presence of voids when prepared with catalysts. With the use of a slow action catalyst, the flexural strength and modulus of the cured phenolic resin were decreased

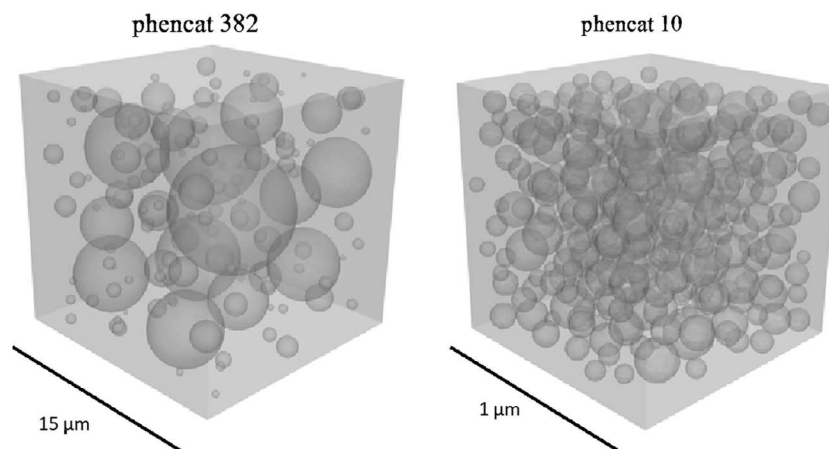


**Figure 7.** The microstructural representations of phenolic resin cured with a slow action catalyst (Phencat 382) (~150 individual microvoids) and a fast action catalyst (Phencat 10) (~300 individual microvoids). Each model has an overall solid density of 70%.

to  $47 \pm 8$  MPa and  $2.0 \pm 0.25$  GPa, respectively. The presence of the voids in the cured resin increases the pressure on the surrounding resin and also they act as stress concentrators rendering the material more fragile.<sup>42,43</sup> When the sample is subjected to a load, stress and strain concentrations will be generated around the voids causing a local plastic deformation. Then with increasing load, cracks will be initiated and grow in the voids-free resin zones, with the resultant reduction in the resin strength.<sup>44,45</sup> Such cracks were clearly observed by SEM image as shown in Figure 2(d).

However, it is important to point out that the average values of the flexural strength ( $68 \pm 12$  MPa) and the flexural modulus ( $2.3 \pm 0.43$  GPa) of the phenolic resin cured with a fast action catalyst were higher than those of phenolic resin cured with a slow action catalyst. Moreover, some of the tested samples from

the phenolic resin cured with a fast action catalyst showed very close or even the same flexural strength values as some of phenolic resin cured without a catalyst (see Supporting Information Table S3 and Figure S1). By taking into account the void volume fraction, it has been noted that the flexural strength of the phenolic resin cured with a fast action catalyst was similar to the flexural strength of the reference sample (cured without catalyst). Whereas in the case of using a slow action catalyst, the flexural strength remains lower than that of reference and fast action cured samples.

Therefore, the differences in the flexural properties between the two phenolic resins (cured with either slow or fast action catalyst) can be attributed to both the structural and chemical changes presented in this article. In terms of the chemical changes, it is possible that the presence of high prevalence methylene bridges

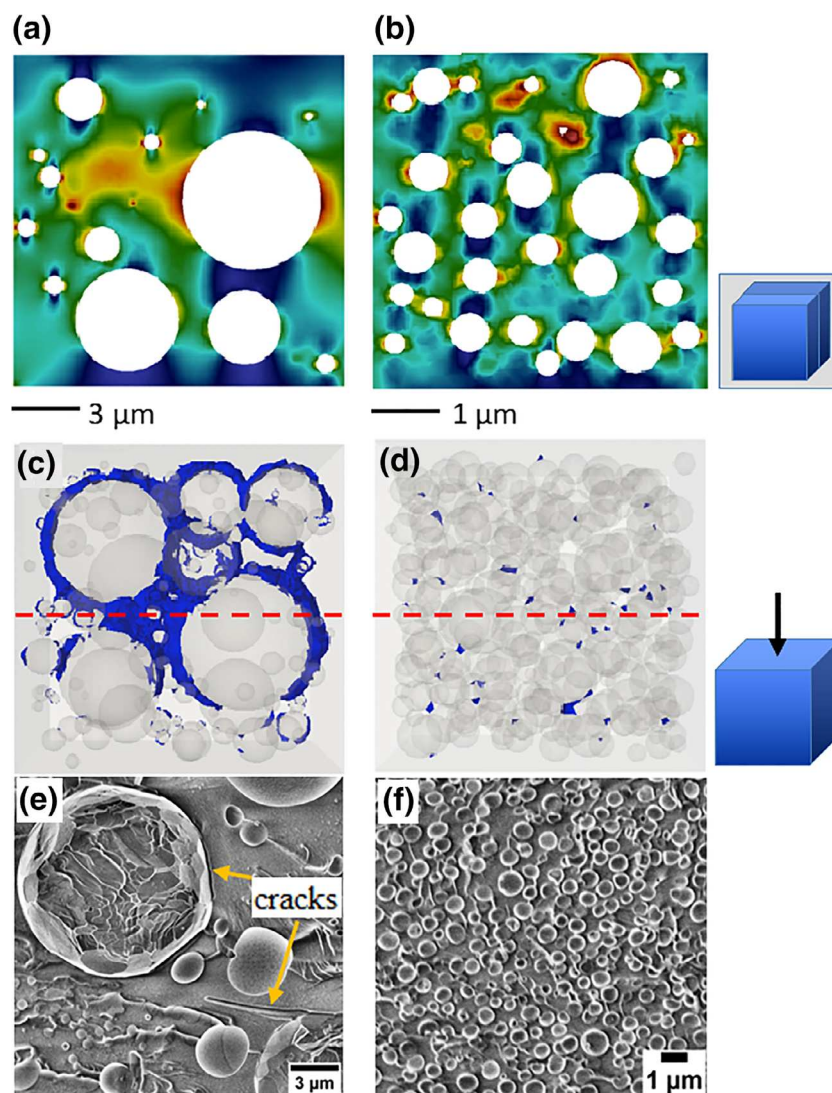


**Figure 8.** The comparison of the stress distribution in models that represent phenolic resin cured with a slow action catalyst (phenocat 382) (a,c) and phenolic resin cured with a fast action catalyst (phenocat 10) (b,d). The resulting von-Mises stress is plotted (a,b) as a cross section of the cube. Red indicates a stress of 88 MPa, while blue indicates a minimum stress of 0. Parts (c) and (d) are top down views of the model highlight only the top 20% of stresses (70–88 MPa) within the system. The red-dashed line indicates the cross section seen in parts (a) and (b). Parts (e) and (f) are the SEM micrographs of the fracture surface of the phenolic cured with slow action catalyst and fast action catalyst, respectively. The small images to the right of the figure highlight the direction of the image seen. [Color figure can be viewed at [wileyonlinelibrary.com](http://wileyonlinelibrary.com)]

in the case of using a fast action catalyst (as discussed within FTIR analysis in section 3.2) could potentially improve the flexural properties of the cured resin. But more significantly, it can be confirmed that the increase in the flexural properties in the case of using fast action catalyst were due to the void size and distribution in the cured resin. For instance, in phenolic foams, it has been found that the cell size and cell distribution have significant effects on the final mechanical properties of the foam. Smaller and more uniform cell size in the final cured foam will potentially improve the mechanical properties.<sup>24</sup> Similarly, in this study, the LV-SEM micrograph and image analysis of the fracture surface of the phenolic resin cured with a fast action catalyst shows small and uniform void diameter distribution, whereas a non-uniform void diameter distribution was observed in the case of using slow action catalyst (see section 3.1).

To understand this further, it was thus confirmed that the void diameter distribution plays a major role in the crack initiation and propagation. Small cracks terminated at both ends by voids were observed in the fracture surface of phenolic resin cured with a fast action catalyst. It was assumed that the small and uniform distances between the small voids can help to prevent the crack propagation in the void-free resin. This is in contrast, to the cracks in the case of using a slow action catalyst was fewer and longer cracks exist, which are seen by SEM in Figure 2(d) to propagate in the void-free area and also along the large voids. Moreover, the long boundary between the void-free area and the large voids is also expected to accelerate the crack growth and hence the early sample failure. All the above were further confirmed by the model in section 3.4.

### Finite Element Modeling

To study the effect of the void size and distribution of phenolic resin cured with slow and fast action catalyst has upon the stress concentration and ultimately the failure strength of the resins, we employ a simplistic finite element model. Experimental void sizes calculated in Figure 3 are directly implemented into a finite element model using an approach previously used to study the effect of electric field enhancement in electro-ceramic materials.<sup>46</sup> Treating the voids as hard spheres, the lists of diameters are randomized and then sequentially positioned randomly into a cube. This process continues until the effective density of the solid is reduced to 70% (assuming both materials have the same voids area fraction [30%] for simplification). These spheres are then subtracted from the solid cube to form the semidense structure replicated the two materials. Due to the differences in size and number of voids for each system (as already seen in SEM images [section 3.1]), the size of the cube is modified to save computation time. Hence, to create models for phenolic resin cured with a fast action catalyst requires approximately 300 voids in a cube of  $5\mu\text{m}^3$ , while for phenolic resin cured with a slow action catalyst, approximately 150 voids in a cube of  $15\mu\text{m}^3$  are need to generate a 70% dense solid. An example for each model can be seen in Figure 7.

The models are then imported into COMSOL<sup>47</sup> and solved using the structural module. We assume the resin Young's modulus is 3.2 GPa with a Poisson's ratio of 0.3.<sup>48</sup> The model assumes the resin is entirely elastic and isotropic. Due to the simplicity in performing the model with the tensile load instead of the bending load, we apply a tensile load of 21 MPa on the top surface as a

reference. This value is chosen as it generates a maximum stress in both samples of approximately 88 MPa, the failure point of the microvoid-free sample. The bottom surface was restricted in movement within plane and a single node in the center of the surface fixed rigidly in all dimensions to not overly constrain the system. Symmetry was employed on the other four surfaces to replicate a central region of "bulk"-like material. The model was then discretised with over two-million tetrahedron elements, ensuring convergence of the results. Figure 8 shows von-Mises stress, highlight in red, the points at which failure may begin. In Figure 8(a), it can be seen that the representation of phenolic resin cured with a slow action catalyst (phencat 382) generates significant stresses between the large voids (over 70 MPa), which extends over a few micrometers in length. This is in comparison to phenolic resin cured with a fast action catalyst (phencat 10) where stresses are as great but highly localized between the small particles and typically restricted to less than 1  $\mu\text{m}$  in length due to the proximity of the voids [Figure 8(b)]. To highlight this further, we plot only the stresses greater than 70 MPa in Figure 8(c,d) as a top-down view. It is clearly visible that for phenolic resin cured with a slow action catalyst high stresses are located around the circumference of larger voids in relation to the applied stress [Figure 8(c)] and extend through the system to other large voids. The same high stresses in phenolic resin cured with a fast action catalyst are only found between two closely placed voids [Figure 8(d)]. If the yield strength of the material is considered to be the point at which a crack would form and spread, it is clear that for phenolic resin cured with a fast action catalyst, these cracks would be between neighboring voids, traveling less than 1  $\mu\text{m}$ . Conversely, for phenolic resin cured with a slow action catalyst, due to the increased distance between voids, the crack could propagate much further, and as such reach a critical point for fracture earlier. This is clearly consistence with the SEM micrographs shown in Figure 8(e,f) and also in good agreement with the flexural property results in section 3.3 (Table II).

### CONCLUSIONS

LV-SEM combined with the finite element modeling suggests that the size and spatial distribution of the voids in the cured phenolic resin are of great importance in determining the final mechanical properties of the resin. While the conventional approach in phenolic resins is to minimize or to avoid the void content in the cured resin, here we show that for the similar void content, achieving a homogenous void distribution is critical. More attention should be paid to the engineering of voids size and distribution. With the use of fast action catalyst in curing the resole phenolic resins, a better balance between the properties and cure cycle could be achieved.

### ACKNOWLEDGMENTS

Sameer F. Hamad gratefully acknowledges the Iraqi Ministry of Higher Education and Scientific Research and its representative in the UK, the Iraqi Cultural Attaché for the financial support. C. Rodenburg thanks the Engineering and Physical Sciences Research Council (EPSRC) for funding under EP/N008065/1. Nicholas Farr thanks EPSRC for funding of his doctoral training studentship. Joel P. Foreman thanks Peter Willson at Caleb Technical Products for providing the resin.

## REFERENCES

1. Wang, J.; Zhang, Y. F. *Polym. - Plast. Technol. Eng.* **2012**, *51*, 1213.
2. Ratna, D.; Karger Kocsis, J. *J. Appl. Polym. Sci.* **2013**, *127*, 4039.
3. Wang, J.; Jiang, H.; Jiang, N. *Thermochim. Acta.* **2009**, *496*, 136.
4. Budiono, H. S.; Surojo, E.; Muhayat, N.; Raharjo, W. W. *MATEC Web Conf.* **2018**, *159*, 1.
5. Der Wu, H.; Lee, M. S.; Wu, Y. D.; Su, Y. F.; Ma, C. C. M. *J. Appl. Polym. Sci.* **1996**, *62*, 227.
6. Alkan, Ü. B.; Kızılcan, N. *Procedia - Soc. Behav. Sci.* **2015**, *195*, 2067.
7. Zhang, Y.; Shen, S.; Liu, Y. *Polym. Degrad. Stab.* **2013**, *98*, 514.
8. Niu, M.; Wang, G. *Cell. Polym.* **2013**, *32*, 155.
9. Yu, Y.; Wang, Y.; Xu, P.; Chang, J. *Materials (Basel)*. **2018**, *11*, 2228.
10. Asim, M.; Saba, N.; Jawaid, M.; Nasir, M.; Pervaiz, M.; Alothman, O. Y. *Curr. Anal. Chem.* **2018**, *14*, 1.
11. Li, J.; Zhu, W.; Zhang, J.; Zhang, S.; Gao, Q.; Li, J.; Zhang, W. *J. Appl. Polym. Sci.* **2019**, *136*, 1.
12. Pupin, C.; Ross, A.; Dubois, C.; Rietsch, J.; Ruiz, E. *Compos. Part A.* **2017**, *100*, 294.
13. Natali, M.; Kenny, J.; Torre, L. *Compos. Sci. Technol.* **2010**, *70*, 571.
14. Sulaiman, S.; Yunus, R.; Ibrahim, N. A.; Rezaei, F. *J. Eng. Sci. Technol.* **2008**, *3*, 79.
15. Manikandan, G. N.; Bogeshwaran, K. *ChemTech Res.* **2016**, *9*, 30.
16. Singh, K. P.; Palmese, G. R. *J. Appl. Polym. Sci.* **2004**, *91*, 3096.
17. De Medeiros, E. S.; Agnelli, A. M.; Joseph, K.; De Carvalho, L. H. *J. Appl. Polym. Sci.* **2003**, *90*, 1678.
18. Parameswaran, P. S.; Bhuvaneshwary, M. G.; Thachil, E. T. *J. Appl. Polym. Sci.* **2009**, *113*, 802.
19. Kaynak, C.; Tasan, C. C. *Eur. Polym. J.* **2006**, *42*, 1908.
20. He, L.; Han, R.; Zhang, Y. *J. Adhes. Sci. Technol.* **2009**, *23*, 1639.
21. Park, B. D.; Riedl, B.; Hsu, E. W.; Shields, J. *Polymer (Guildf)*. **1999**, *40*, 1689.
22. Singh, A.; S. Aggrawal; D. Lal. *Def. Sci. J.* **2019**, *69*, 46–52.
23. Aierbe, G. A.; Echeverria, J. M.; Martin, M. D.; Mondragon, I. *Polymer (Guildf)*. **1998**, *39*, 3467.
24. Mougel, C.; Garnier, T.; Cassagnau, P.; Sintès-Zydowicz, N. *Polymer (Guildf)*. **2019**, *164*, 86.
25. Li, Q.; Chen, L.; Li, X.; Zhang, J.; Zheng, K.; Zhang, X.; Tian, X. *J. Appl. Polym. Sci.* **2016**, *133*, 1.
26. Wolfrum, J.; G. W. Ehrenstein. *J. Appl. Polym. Sci.* **1999**, *74*, 3173.
27. Astarloa Aierbe, G.; Echeverría, J. M.; Martin, M. D.; Etxeberria, A. M.; Mondragon, I. *Polymer (Guildf)*. **2000**, *41*, 6797.
28. Lin, C. C.; Teng, H. *Ind. Eng. Chem. Res.* **2002**, *41*, 1986.
29. Hu, X.-M.; Zhao, Y.-Y.; Cheng, W.-M. *Polym. Compos.* **2015**, *36*, 1531.
30. Monni, J.; Alvila, L.; Pakkanen, T. T. *Ind. Eng. Chem. Res.* **2007**, *46*, 6916.
31. Loustalot, M. F. G.; Larroque, S.; Grande, D.; Grenier, P. *Polymer (Guildf)*. **1996**, *37*, 1363.
32. St. John, N. A.; Brown, J. R. *Compos. Part A Appl. Sci. Manuf.* **1998**, *29*, 939.
33. Spurr, R. A.; Erath, E. H.; Myers, H.; Pease, D. C. *Ind. Eng. Chem.* **1957**, *49*, 1839.
34. Izumi, A.; Nakao, T.; Iwase, H.; Shibayama, M. *Soft Matter.* **2012**, *8*, 8438.
35. Borkovec, M.; Paris, W. D. E. *Appear. Fractals.* **1994**, *2*, 521.
36. Zhang, A.; Bai, H.; Li, L. *Chem. Rev.* **2015**, *115*, 9801.
37. Ku, H. S. L.; Cardona, F.; Trada, M.; Vigier, G. *J. Appl. Polym. Sci.* **2009**, *114*, 1927.
38. Schindelin, J.; Arganda-Carreras, E.; Frise, I.; Kaynig, V.; Longair, M.; Pietzsch, T.; Preibisch, S.; Rueden, C.; Saalfeld, S.; Schmid, B.; Tinevez, J.-Y.; White, D. J.; Hartenstein, V.; Eliceiri, K.; Tomancak, P.; Cardona, A. *Nat. Methods.* **2012**, *9*, 1.
39. Poljanšek, I.; Krajnc, M. *Acta Chim. Slov.* **2005**, *52*, 238.
40. Jähnigen, S.; Brendler, E.; Böhme, U.; Heide, G.; Kroke, E. *New J. Chem.* **2014**, *38*, 744.
41. Parameswaran, P. S.; Thachil, E. T. *Int. J. Polym. Mater. Polym. Biomater.* **2007**, *56*, 177.
42. Brown, J.; Mathys, Z. *J. Mater. Sci.* **1997**, *32*, 2599.
43. Feih, S.; Mathys, Z.; Mathys, G.; Gibson, A. G.; Robinson, M.; Mouritz, A. P. *Polym. Degrad. Stab.* **2008**, *93*, 376.
44. Aratama, S.; Hashizume, R.; Takenaka, K.; Koga, K.; Tsumura, Y.; Miyake, T.; Nishikawa, M.; Hojo, M. *Adv. Compos. Mater.* **2016**, *3046*, 1.
45. Paskaramoorthy, R.; Bugarin, S.; Reid, R. G. *Int. J. Solids Struct.* **2011**, *48*, 2255.
46. Dale, G.; Strawhorne, M.; Sinclair, D. C.; Dean, J. S. *J. Am. Ceram. Soc.* **2018**, *101*, 1211.
47. COMSOL. Multiphysics® Modeling Software. <https://uk.comsol.com/> (accessed 18 April 2019).
48. Arnold, S. M.; Murthy, P. L.; Bednarczyk, B. A.; Lawson, J. W.; Monk, J. D. *NASA Tech. Memo.* **2016**, *219124*, 1.